

# Efficient fault-tolerant implementations of non-Clifford gates with reconfigurable atom arrays

Yi-Fei Wang,<sup>1</sup> Yixu Wang,<sup>1</sup> Yu-An Chen,<sup>2</sup> Wenjun Zhang,<sup>3</sup> Tao Zhang,<sup>3</sup>  
Jiazhong Hu,<sup>3,4</sup> Wenlan Chen,<sup>3,4</sup> Yingfei Gu,<sup>1,\*</sup> and Zi-Wen Liu<sup>5,†</sup>

<sup>1</sup>*Institute for Advanced Study, Tsinghua University, Beijing 100084, China*

<sup>2</sup>*International Center for Quantum Materials, School of Physics, Peking University, Beijing 100871, China*

<sup>3</sup>*Department of Physics and State Key Laboratory of Low Dimensional  
Quantum Physics, Tsinghua University, Beijing 100084, China*

<sup>4</sup>*Frontier Science Center for Quantum Information and Collaborative  
Innovation Center of Quantum Matter, Beijing, 100084, China*

<sup>5</sup>*Yau Mathematical Sciences Center, Tsinghua University, Beijing 100084, China*

(Dated: December 15, 2023)

To achieve scalable universal quantum computing, we need to implement a universal set of logical gates fault-tolerantly, for which the main difficulty lies with non-Clifford gates. We demonstrate that several characteristic features of the reconfigurable atom array platform are inherently well-suited for addressing this key challenge, potentially leading to significant advantages in fidelity and efficiency. Specifically, we consider a series of different strategies including magic state distillation, concatenated code array, and fault-tolerant logical multi-controlled- $Z$  gates, leveraging key platform features such as non-local connectivity, parallel gate action, collective mobility, and native multi-controlled- $Z$  gates. Our analysis provides valuable insights into the efficient experimental realization of logical gates, serving as a guide for the full-cycle demonstration of fault-tolerant quantum computation with reconfigurable atom arrays.

## INTRODUCTION

The implementation of reliable large-scale quantum computing holds great promise for significant technological advancements but poses substantial challenges in practice, as quantum systems are inherently susceptible to noise and errors. A crucial idea for tackling this problem is quantum error correction (QEC) [1–3], wherein the central element is quantum codes that encode the logical information of quantum systems. Logical error rates can be suppressed by the error detection and correction procedure. To implement large-scale general-purpose quantum computation in practice, we further need to be able to execute a universal set of quantum gates at the level of logical qubits fault-tolerantly. The most straightforward fault-tolerant logical gates are those implemented by transversal gates upon codes, which take the form of tensor products of gates acting on disjoint physical subsystems like individual code qubits. Unfortunately, a no-go theorem of Eastin and Knill [4] states that transversal operators on any nontrivial QEC code cannot be universal, which calls for other approaches for fault-tolerant (FT) logical gates. In general, Clifford gates represent the “easy” part—they can be classically simulated efficiently [1, 5] and are relatively straightforward to protect and implement fault-tolerantly. However, to achieve universal quantum computation, it is necessary to include non-Clifford gates such as  $T$  and  $CCZ$  gates, which represent the main bottleneck. To address this problem, multiple frameworks have been proposed and developed, including magic state distillation (MSD) [6–9], code concatenation [10, 11], and code switching [12, 13].

From a practical viewpoint, FT implementation of non-Clifford logical gates faces fundamental obstacles when the system architecture or interaction is restricted to two spatial dimensions (2D) or lower, which is more feasible in various experimental platforms. In particular, it is well known that for 2D stabilizer codes [18] (such as the surface code [19–21] which has been a leading candidate for realizing fault tolerance) and even subsystem codes [22], gates that can be implemented transversally or indeed with constant-depth quantum circuits are restricted to the Clifford group. As a result, the implementation of non-Clifford gates, which are required for universality, is expected to be difficult with 2D locality due to the necessity of long-range interactions. Here, we consider the reconfigurable atom array quantum processor [16], an emerging hardware architecture [23, 24] that enables highly parallel and dynamically all-to-all gates, thereby overcoming the aforementioned geometric locality constraint.

Specifically, we propose and analyze several hardware-efficient schemes for fault-tolerantly implementing non-Clifford gates with reconfigurable atom arrays. The primary ones that we will elaborate on include magic state distillation, concatenated code array, and FT logical multi-controlled- $Z$  gates. Remarkably, all of these approaches capitalize on certain characteristic features of the atom array experimental platform, particularly the reconfigurability and parallel efficient control, which enable significant advantages; see Table I for a summary. We will describe the implementation methods and analyze their experimental feasibility in detail, from which it will become evident how the native features of the

	Non-local connectivity	Parallel gate action	Collective mobility	Native multi-controlled-Z
Magic state distillation	✓	✓	✓	
Concatenated code array	✓	✓	✓	
FT multi-controlled-Z codes	✓	✓	✓	✓

TABLE I. Summary of the major schemes for the efficient fault-tolerant implementation of non-Clifford gates considered in this article and the characteristic features of the reconfigurable atom array platform that can significantly enhance their efficiency. The rows correspond to different schemes for fault-tolerant non-Clifford gates, and the columns correspond to features of the reconfigurable atom array platform. Here, non-local connectivity refers to the reconfigurable architecture that allows non-local gates [14]; parallel gate action refers to the parallel grid illumination that realizes parallel single qubit rotations [15, 16]; collective mobility refers to the transport of multiple qubits via moving 2D acousto-optic deflectors (AOD), which can be used to perform parallel entangling CZ gates in a zone with global Rydberg excitation laser [17]; native multi-controlled-Z refers to the experimental realization of a multi-qubit gate by moving multiple atoms into Rydberg blockade regime, e.g. CCZ by preparing three atoms in the nearest-neighbor blockade regime [17].

platform are particularly favorable for implementing non-Clifford gates.

### MAGIC STATE DISTILLATION

Magic state distillation (MSD) and injection constitutes a major approach to achieve FT universal logical gates. Roughly speaking, the protocol refers to the procedure of distilling certain non-stabilizer states to arbitrary fidelity from noisy states (which may have suffered from storage error) offline, and directly “injecting” them into the circuit to realize non-Clifford gates [6], both steps using only Clifford gates. This method is based on assuming ideal Clifford gates as their fault tolerance can be achieved straightforwardly, and focus on dealing with noisy non-Clifford resources.

Here we consider the  $T$  gate (i.e.  $T = \exp(-i\pi\sigma^z/8)$ ), which is a standard non-Clifford gate forming a universal gate set together with Clifford gates. It can be implemented with the ancilla  $|T\rangle = |0\rangle + e^{i\pi/4}|1\rangle$  as shown in Fig. 1(a). The  $[[15, 1, 3]]$  quantum Reed-Muller (QRM) code has transversal logical  $T$  gates and can be used to distill the ancilla. We consider the distillation scheme (shown in Fig. 1(b)) which consumes 15 noisy ancillae and outputs 1 more accurate ancilla: an EPR pair  $(|00\rangle + |11\rangle)/\sqrt{2}$  is prepared and one qubit is encoded into the 15-qubit code. Then a transversal  $T$  gate is applied using the input noisy ancillae. Finally, all 15 qubits are measured in the  $X$  basis. If any of the four  $X$  stabilizers is not satisfied, the output will be discarded, otherwise one may apply a  $Z$  operator conditioned on the product of all  $X$  measurements which is exactly the logical  $\bar{X}$  measurement [25].

Ideally, we would like to carry out magic state distillation on a logical level such that qubits in circuit 1(b) are protected by quantum codes, that is, all the “qubit” in the previous paragraph refers to logical qubit encoded in some codes (for example surface codes). The fault-tolerant universal quantum computation architecture using this logical level distillation is shown in Fig. 1(c). A more feasible short-term goal is to distill  $T$  ancillae on a

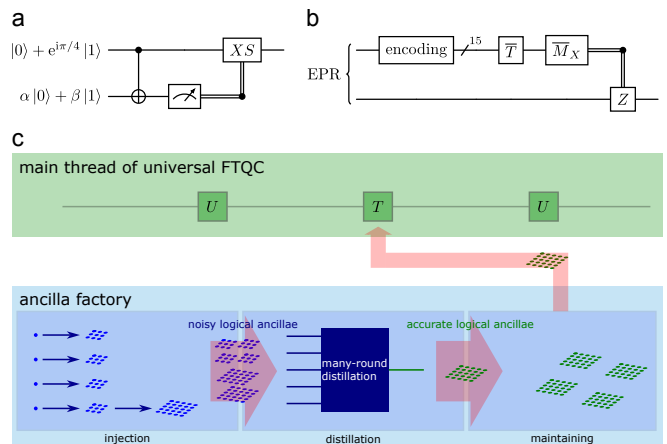


FIG. 1. (a) The circuit for applying a  $T$  gate with an ancilla. Note that the input qubit is destructively measured and the ancillary qubit serves as the output. (b) Illustration of magic state distillation. One qubit of an entangled pair is encoded into the  $[[15, 1, 3]]$  quantum Reed-Muller code and a logical  $T$  gate is applied via  $T^\dagger$  gates on each qubit. Each  $T^\dagger$  gate is implemented using a noisy ancilla. After measurement on the 15-qubit code and a conditioned  $Z$  on the other qubit of the EPR pair, the latter qubit is transformed to a more accurate ancilla. (c) Universal fault-tolerant quantum computation (FTQC) with magic state distillation. An ancilla factory is constantly injecting required ancilla to QEC codes of various sizes, which are then used for many-round distillation until the required fidelity is achieved. The produced ancillae are then maintained by standard error correction procedure for quantum memory. When a logical  $T$  is required in the main thread of the computation, a good ancilla is moved out from the factory to the computation region.

physical level, as a demonstration of both the distillation scheme and the experiment techniques.

For physical level distillation, since the  $[[15, 1, 3]]$  QRM code is intrinsically a 3D code, it is inefficient to implement the encoding using local gates in 2D geometry. The reconfigurability of atom arrays provides a significant advantage. For the distillation circuit in Fig. 4 in Appendix A, 35 CNOT gates are required for EPR preparation and encoding. If the qubits are fixed in a

low-dimensional architecture we need many swap gates to implement long-range CNOT gates. This will not only take more time but also introduce more errors. As for the distillation at logical level using surface code, non-local logical CNOT gates between two surface codes are required. Even if lattice surgery techniques [26] are used to implement logical CNOT gate locally between adjacent code blocks, the non-locality in the distillation circuit still requires the additional logical swaps, each using 3 CNOT gates by lattice surgery, making the overhead much larger.

In reality, the Clifford gates are erroneous. The errors are highly biased in the reconfigurable atom array platform [27]. As for Pauli errors, the most probable error is the  $Z$  error for two-qubit CZ gates, while idling error and single qubit error are much smaller. At the logical level, physical error rates below threshold are suppressed exponentially. Therefore, as a demonstration of the viability of the experiment, we analyze only the impact of logical  $Z$  errors in the CZ gates. Once an error occurs, it propagates through the circuit. If the error does not spread out, it will lead to a single-site error in the 15-qubit code, which can be detected and corrected by stabilizer measurements. As a result, this kind of error will just decrease the rate of success (that is, the rate of distillation rounds that all stabilizers are satisfied). Only 3 non-spread errors occurring simultaneously that happen to form a logical operator can decrease the output fidelity. The contribution to the output error from such circumstances is then proportional to  $p^3$  given the Clifford error rate  $p$ . On the other hand, if an error spreads to a logical error, the dependence of output noise on the rate of this kind of error is linear, but the rate of success is not affected. Finally, error happening on the output qubit when creating the EPR pair in Fig. 1 (b) comes directly into the final output. Based on the above analysis, we find that there are 5 “key” CZ gates (see Fig. 4), whose errors will propagate to a logical  $S^1$  operator, contributing to the leading order output error. If these key gates have gate fidelity  $(1 - q)^2$ , (that is, a  $Z$  error can occur on each qubit with probability  $q$  when applying the gate), while other CZ gates have fidelity  $(1 - p)^2$ , the leading order of the output error is  $3.5q$ .

We simulate one distillation round 100 times at different input ancilla noise and CZ gate fidelity. Fig. 2 (a, b) reveal the performance of MSD when all CZ gates have the same gate fidelity, which can serve as a reference for near-term experiments. Especially at CZ gate fidelity 99.5%, which is the record of today’s physical gate fidelity, one can achieve break-even when input fidelity is larger than 1% ( $\gtrsim 0.75\%$  according to our analytical result). Note that since 1% is much larger than the error of single-qubit rotation for recent techniques, distillation at a physical level is more a proof of principle demonstration than a practical procedure. Fig. 2 (c, d) is more surprising: when the input noise is 2%, a point

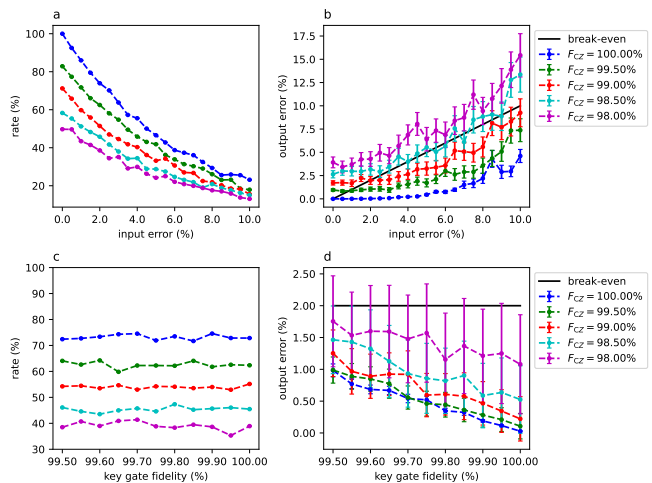


FIG. 2. Effect of two-qubit gate error on distillation of  $T$  gates obtained from Monte Carlo simulation. (a, b) Rate of successful rounds and output noise as a function of input noise, under different fidelities (“ $F_{CZ}$ ” in legend) of two-qubit CZ gates with independent  $Z$  errors on each qubit. Break-even condition that output noise equals to input noise is indicated by the black solid line in (b). (c, d) Rate of successful rounds and output noise as a function of key gate fidelity (see main text), under different fidelities of other CZ gates.

at which 99% CZ fidelity achieves break-even (b), only by improving the fidelity of 5 key gates to 99.5% can we achieve break-even when all other CZ gates still have the fidelity of 98%. This manifests our analysis that the output fidelity is linearly dependent on key gate fidelity, indicating that at the logical level, 5 key CZ gates need to be protected using larger codes while smaller codes suffice for other gates. We believe that this property, ensured by the biased error property of the platforms, can lower the overhead of distillation significantly.

The above error propagation analysis indicates that the output error is dominantly contributed by errors on two qubits. This motivates us to flag method [28, 29] to monitor whether errors occur on these qubits during a given circuit sequence. The flag qubit gadget is equivalent to the original distillation circuit in the case where no error occurs within the monitored sequence. If a  $Z$  error indeed occurs on the monitored qubit, it will propagate to the flag qubit and cause it to flip. If a flip is detected on the flag qubit, the process is discarded and we start over. If no flip is detected, we believe no  $Z$  error occurs and proceed with further gates and syndrome detection process. As errors may occur in the gates of the flag gadgets as well as the measurement of the flag qubits, there is a possibility that  $Z$  errors indeed occur in the monitored circuit sequence but the flag qubit fails to detect it. Nevertheless, this requires at least two uncorrelated errors happening. Therefore, adding flag qubit gadgets could suppress the output error proportional to  $pq$ , instead of  $q$  in the original distillation circuit. We

provide an explicit construction of such a flag gadget in Fig. 5.

### CONCATENATED CODE ARRAY

Code concatenation provides another way to circumvent the Eastin–Knill theorem to achieve universal FT gates particularly fit for the atom array platform, the essential idea of which is to “combine” different FT gate sets of different codes [10]. Consider two codes  $\mathcal{C}_1$  and  $\mathcal{C}_2$  such that the union of their transversal gate sets is universal. We concatenate these two codes such that each physical qubit in  $\mathcal{C}_1$  is encoded as a logical qubit for  $\mathcal{C}_2$ . For a small example, we can take  $\mathcal{C}_1$  to be the  $[[7, 1, 3]]$  Steane code and  $\mathcal{C}_2$  the  $[[15, 1, 3]]$  QRM code [10].  $\mathcal{C}_1$  has transversal gate set  $\{H, S, \text{CNOT}\}$  while  $\mathcal{C}_2$  has transversal gate set  $\{T, \text{CNOT}\}$ . We can arrange the physical qubits into a  $7 \times 15$  array, with each row forming the 15-qubit code while the collection of rows corresponding to the 7-qubit code; see Fig. 3. To implement a logical  $S$  or CNOT, we can apply the gate qubit-wise: a qubit-wise  $S$  is a logical  $S^\dagger$  for the 15-qubit code, and a qubit-wise  $S^\dagger$  is a logical  $S$  for the 7-qubit code; similar is the CNOT gate. To implement a logical  $T$ , which is not transversal for the 7-qubit code, we need to apply 4 CNOT gates and 1  $T$  gate at the physical level of the 7-qubit code, which are transversal for the 15-qubit code: errors can only propagate within individual columns. To implement a logical  $H$ , which is transversal for the 7-qubit code but not transversal for the 15-qubit code, we need to apply a logical  $H$  gate, which amounts to 14 CNOT gates and 1  $H$  gate, for each 15-qubit code: errors can only propagate within individual rows [30]. Both  $\mathcal{C}_1$  and  $\mathcal{C}_2$  have distance 3 but neither has a transversal universal gate set. Nevertheless, we can implement a universal gate set fault-tolerantly in the concatenated code with an effective distance of 3.

The parallel gate action and the collective mobility features of the atom arrays are ideal for implementing a concatenated code array scheme. For instance, in the logical  $T$  and  $H$  implementation, CNOT gates between two rows or columns can be performed in parallel via transport-based entangling gates [14], see Fig. 3 for details. To demonstrate the experimental feasibility, we give an estimation for the time cost of logical  $T$  and  $H$  based on the architecture and technology demonstrated in [14], utilizing a system of acoustic optical deflectors (AOD). This system enables a simultaneously movement of an entire row or column of the tweezers array. In the atom arrays, two atoms are separated by roughly  $10 \mu\text{m}$ . Two adjacent sites in static tweezer are separated by less than  $2 \mu\text{m}$ . The moving speed of atoms at which the fidelity is well preserved is roughly  $0.5 \text{ m/s}$ . The typical moving time is then at the order of some  $20 \mu\text{s}$ . Besides moving at a constant velocity there are other processes includ-

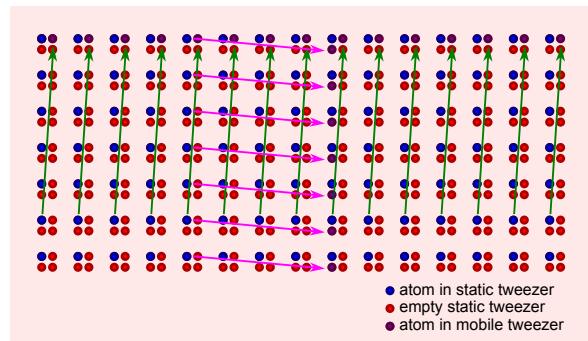


FIG. 3. Parallel implementation of a universal set of logical gates by code concatenation. A logical qubit is encoded in the  $[[7, 1, 3]]$  Steane code concatenated with the  $[[15, 1, 3]]$  QRM code forming a  $7 \times 15$  atom array (dark blue circles) held by an array of static tweezers generated with a spatial light modulator (SLM, red circles), where each row is a 15-qubit code and a physical “qubit” for the 7-qubit code. The array of static tweezers are positioned as a lattice with 4-site cells, whose lattice constant is larger than the Rydberg blockade radius of the atom, but the distance of two adjacent sites in one cell is less than the Rydberg blockade radius. To apply CNOT gates transversally between two rows, say rows 1 and 6, one can use an array of mobile tweezers generated with AOD to shift one row of atoms to the neighbor sites of the other row (green arrow). One then turns off the tweezers, applies a row of Hadamard gates on the target line, turns on a pulse to apply CZ gates on the atom pairs closer than the Rydberg blockade radius simultaneously, and applies Hadamard gates on the target line again. To apply CNOT gates transversally between two columns, say columns 5 and 9, one can move one column of atoms to the neighbor of the other (purple arrow). The other operations are similar.

ing the acceleration which has minor influence on time cost, the pulse implementing CZ gates which lasts for roughly  $200 \text{ ns} \ll 20 \mu\text{s}$ , and transferring between spatial light modulator (SLM) and AOD tweezers which takes roughly  $100 \sim 200 \mu\text{s}$  [16]. Only the last procedure is relevant to our time estimation. For logical  $T$  gate, 4 cycles of CNOT gates are needed [10, 30], involving row movements  $R_7(7 \rightarrow 6), R_6(6 \rightarrow 1), R_6(1 \rightarrow 6), R_7(6 \rightarrow 7)$ , where  $R_i(j \rightarrow k)$  means moving the  $i$ th row of atoms from row  $j$  to row  $k$ , taking roughly  $20 \mu\text{s}, 100 \mu\text{s}, 100 \mu\text{s}, 20 \mu\text{s}$ , respectively, adding up to  $0.24 \text{ ms}$  for moving only and  $0.84 \text{ ms}$  with transferring time included (taking transferring time as  $150 \mu\text{s}$ ). For logical  $H$  gate, 8 cycles of CNOT gates are needed [30]. In the worst case that after each step columns are moved back to its original position, it takes roughly  $3.76 \text{ ms}$  to implement the logical  $H$  gate, comparing to an order of seconds for the decoherence time of an atom qubit. The time cost can be further reduced by optimizing the moving strategy based on different computational task at a software level, as well as using time optimal control techniques at a hardware level.

One advantage of the reconfigurable atom array platform is the natural physical implementation of multi-controlled- $Z$  gates, denoted by  $C^m Z$  where  $m$  is the number of control qubits, which are non-Clifford when  $m \geq 2$ . Due to this feature, we are tempted to consider  $C^m Z$  gates which are suited to certain important scenarios (e.g., generating hypergraph states [31] which are representative many-body entangled magic states [32]) and generally provide an alternative choice of non-Clifford gates for circuit compilation.

Stabilizer codes based on triorthogonal matrices, such as the  $[[15, 1, 3]]$ ,  $[[49, 1, 5]]$ , and a family of  $[[3k + 8, k, 2]]$  triorthogonal codes, support logical CCZ gates implemented by transversal physical CCZ gates [7, 33]. Additionally, the 3D surface code on the rectified cubic lattice, which exhibits a similar triorthogonal structure, has logical CCZ gates implemented by transversal physical CCZ gates [34]. This concept has been further generalized to the 4D octaplex tessellation, enabling the logical CCCZ gate to be implemented by transversal physical CCCZ gates [35]. Generally, the  $D$ -dimensional toric code permits logical non-Pauli gates from the  $D$ -th level of the Clifford hierarchy [18]. The duality between color codes and toric codes [36] enables logical  $C^{D-1} Z$  gates in the  $D$ -dimensional toric code through transversal  $R_m$  gates up to a Clifford circuit, where  $R_D := \text{diag}(1, \exp(2\pi i/2^D))$ , saturating the Bravyi-König bound [18]. Furthermore, we consider the  $D$ -dimensional  $(1, D-1)$ -toric code on the hypercubic tessellation where the physical system consists of one qubit per edge, and the stabilizers are  $X$ -star (product of  $X$  incident at a vertex) and  $Z$ -plaquette (product of  $Z$  around a face) terms. It contains 0-dimensional excitations (i.e., particles) and  $(D-2)$ -dimensional excitations. As discussed in detail in Appendix B, the logical  $C^{D-1} Z$  gates can be implemented fault-tolerantly with a constant-depth circuit of physical  $C^{D-1} Z$  gates. This approach has the advantage that the implementation is straightforward and can be generalized directly to higher dimensions, without the need for intricate higher-dimensional rectifications or tessellations. It is worth emphasizing the suitability of high-dimensional codes and multi-controlled- $Z$  gates for the reconfigurable atom array platform. To achieve universality, we may use such codes in code switching or code concatenation strategies. In this platform, these exotic high-dimensional codes can offer unique implementation advantages and greater flexibility for gate choice, further enhancing their utility in practical quantum computing.

Implementation of non-Clifford gates is costly but indispensable for fault-tolerant universal quantum computation. In this article, we describe how the native features of the reconfigurable atom array platform can lead to unique advantages in fault-tolerantly implementing non-Clifford gates. In particular, we provide detailed analyses for magic state distillation and code concatenation methods. Moreover, motivated by the unique feasibility of multi-controlled- $Z$  gates in this platform, we specifically discuss codes that use them to realize FT logical multi-controlled- $Z$ .

Besides the methods analyzed in detailed in this article, there are other schemes for FT universal gates. A well established one is code switching [12, 37], which enables transversal universal gates through gauge fixing. This approach also inevitably involves codes beyond 2D so the reconfigurability of the atom array is again crucial. It could also be worthwhile to further explore the usage of relevant methods such as flag qubits [28, 29] and just-in-time decoding [38, 39].

On the other hand, it would be valuable to systematically benchmark and compare the resource costs of different approaches for fault tolerance in the reconfigurable atom platform, in light of the comparison between e.g. MSD and code switching with color codes [40] in the literature.

There are numerous other proposals exploring different features for reconfigurable atom array platform, including biased noise [41, 42], erasure error conversion [43] and highly non-local quantum LDPC codes [44]. With the rapid advancements of experimental technologies, now is an opportune time to explore and implement different methods which may pave the way for practical quantum computing.

## ACKNOWLEDGEMENTS

We thank Hui Zhai for comments on the draft and collaborations on related projects. WZ, TZ, JH and WC are supported by National Key Research and Development Program of China (2021YFA0718303, 2021YFA1400904) and National Natural Science Foundation of China (92165203, 61975092, 11974202). YW is supported by Shuimu Tsinghua Scholar Program of Tsinghua University.

---

\* [guyingfei@tsinghua.edu.cn](mailto:guyingfei@tsinghua.edu.cn)

† [zwliu0@mail.tsinghua.edu.cn](mailto:zwliu0@mail.tsinghua.edu.cn)

- [1] M. A. Nielsen and I. L. Chuang, *Quantum Computation and Quantum Information* (Cambridge University Press, 2000).
- [2] P. W. Shor, Scheme for reducing decoherence in quantum computer memory, *Phys. Rev. A* **52**, R2493 (1995).
- [3] D. Gottesman, *Stabilizer Codes and Quantum Error Correction*, Ph.D. thesis, California Institute of Technology (1997).
- [4] B. Eastin and E. Knill, Restrictions on transversal encoded quantum gate sets, *Phys. Rev. Lett.* **102**, 110502 (2009).
- [5] D. Gottesman, The heisenberg representation of quantum computers (1998).
- [6] S. Bravyi and A. Kitaev, Universal quantum computation with ideal clifford gates and noisy ancillas, *Phys. Rev. A* **71**, 022316 (2005).
- [7] S. Bravyi and J. Haah, Magic-state distillation with low overhead, *Phys. Rev. A* **86**, 052329 (2012).
- [8] J. Haah, M. B. Hastings, D. Poulin, and D. Wecker, Magic state distillation with low space overhead and optimal asymptotic input count, *Quantum* **1**, 31 (2017).
- [9] M. B. Hastings and J. Haah, Distillation with sublogarithmic overhead, *Phys. Rev. Lett.* **120**, 050504 (2018).
- [10] T. Jochym-O'Connor and R. Laflamme, Using concatenated quantum codes for universal fault-tolerant quantum gates, *Phys. Rev. Lett.* **112**, 010505 (2014).
- [11] T. J. Yoder, R. Takagi, and I. L. Chuang, Universal fault-tolerant gates on concatenated stabilizer codes, *Phys. Rev. X* **6**, 031039 (2016).
- [12] J. T. Anderson, G. Duclos-Cianci, and D. Poulin, Fault-tolerant conversion between the steane and reed-muller quantum codes, *Phys. Rev. Lett.* **113**, 080501 (2014).
- [13] F. Butt, S. Heußen, M. Rispler, and M. Müller, Fault-Tolerant Code Switching Protocols for Near-Term Quantum Processors (2023), [arXiv:2306.17686 \[quant-ph\]](https://arxiv.org/abs/2306.17686).
- [14] D. Bluvstein, H. Levine, G. Semeghini, T. T. Wang, S. Ebadi, M. Kalinowski, A. Keesling, N. Maskara, H. Pichler, M. Greiner, V. Vuletić, and M. D. Lukin, A quantum processor based on coherent transport of entangled atom arrays, *Nature* **604**, 451–456 (2022).
- [15] T. M. Graham, Y. Song, J. Scott, C. Poole, L. Phuttitarn, K. Jooya, P. Eichler, X. Jiang, A. Marra, B. Grinkemeyer, M. Kwon, M. Ebert, J. Cherek, M. T. Lichtman, M. Gillette, J. Gilbert, D. Bowman, T. Ballance, C. Campbell, E. D. Dahl, O. Crawford, N. S. Blunt, B. Rogers, T. Noel, and M. Saffman, Multi-qubit entanglement and algorithms on a neutral-atom quantum computer, *Nature* **604**, 457 (2022).
- [16] D. Bluvstein, S. J. Evered, A. A. Geim, S. H. Li, H. Zhou, T. Manovitz, S. Ebadi, M. Cain, M. Kalinowski, D. Hangleiter, J. P. B. Ataiades, N. Maskara, I. Cong, X. Gao, P. S. Rodriguez, T. Karolyshyn, G. Semeghini, M. J. Gullans, M. Greiner, V. Vuletić, and M. D. Lukin, Logical quantum processor based on reconfigurable atom arrays, *Nature* (2023).
- [17] H. Levine, A. Keesling, G. Semeghini, A. Omran, T. T. Wang, S. Ebadi, H. Bernien, M. Greiner, V. Vuletić, H. Pichler, and M. D. Lukin, Parallel implementation of high-fidelity multiqubit gates with neutral atoms, *Phys. Rev. Lett.* **123**, 170503 (2019).
- [18] S. Bravyi and R. König, Classification of topologically protected gates for local stabilizer codes, *Phys. Rev. Lett.* **110**, 170503 (2013).
- [19] S. B. Bravyi and A. Y. Kitaev, Quantum codes on a lattice with boundary (1998), [arXiv:quant-ph/9811052 \[quant-ph\]](https://arxiv.org/abs/quant-ph/9811052).
- [20] E. Dennis, A. Kitaev, A. Landahl, and J. Preskill, Topological quantum memory, *Journal of Mathematical Physics* **43**, 4452–4505 (2002).
- [21] A. G. Fowler, M. Mariantoni, J. M. Martinis, and A. N. Cleland, Surface codes: Towards practical large-scale quantum computation, *Phys. Rev. A* **86**, 032324 (2012).
- [22] F. Pastawski and B. Yoshida, Fault-tolerant logical gates in quantum error-correcting codes, *Phys. Rev. A* **91**, 012305 (2015).
- [23] D. Barredo, S. de Léséleuc, V. Lienhard, T. Lahaye, and A. Browaeys, An atom-by-atom assembler of defect-free arbitrary two-dimensional atomic arrays, *Science* **354**, 1021 (2016).
- [24] M. Endres, H. Bernien, A. Keesling, H. Levine, E. R. Anschuetz, A. Krajenbrink, C. Senko, V. Vuletic, M. Greiner, and M. D. Lukin, Atom-by-atom assembly of defect-free one-dimensional cold atom arrays, *Science* **354**, 1024 (2016).
- [25] There is an alternative scheme: encode a  $|+\rangle = (|0\rangle + |1\rangle)/\sqrt{2}$  to the 15-qubit QRM code, apply a transversal  $T$ , and then decode to extract the information in the 15 qubits to one qubit. This scheme uses one less qubit but take twice the number of Clifford gates, which is slower and more sensitive to Clifford errors.
- [26] D. Horsman, A. G. Fowler, S. Devitt, and R. V. Meter, Surface code quantum computing by lattice surgery, *New Journal of Physics* **14**, 123011 (2012).
- [27] S. J. Evered, D. Bluvstein, M. Kalinowski, S. Ebadi, T. Manovitz, H. Zhou, S. H. Li, A. A. Geim, T. T. Wang, N. Maskara, H. Levine, G. Semeghini, M. Greiner, V. Vuletić, and M. D. Lukin, High-fidelity parallel entangling gates on a neutral-atom quantum computer, *Nature* **622**, 268 (2023).
- [28] R. Chao and B. W. Reichardt, Quantum error correction with only two extra qubits, *Phys. Rev. Lett.* **121**, 050502 (2018).
- [29] R. Chao and B. W. Reichardt, Fault-tolerant quantum computation with few qubits, *npj Quantum Information* **4**, 42 (2018).
- [30] C. Chamberland, T. Jochym-O'Connor, and R. Laflamme, Overhead analysis of universal concatenated quantum codes, *Phys. Rev. A* **95**, 022313 (2017).
- [31] M. Rossi, M. Huber, D. Bruß, and C. Macchiavello, Quantum hypergraph states, *New Journal of Physics* **15**, 113022 (2013).
- [32] Z.-W. Liu and A. Winter, Many-body quantum magic, *PRX Quantum* **3**, 020333 (2022).
- [33] A. Paetznick and B. W. Reichardt, Universal fault-tolerant quantum computation with only transversal gates and error correction, *Phys. Rev. Lett.* **111**, 090505 (2013).
- [34] M. Vasmer and D. E. Browne, Three-dimensional surface codes: Transversal gates and fault-tolerant architectures, *Phys. Rev. A* **100**, 012312 (2019).
- [35] T. Jochym-O'Connor and T. J. Yoder, Four-dimensional toric code with non-clifford transversal gates, *Phys. Rev. Res.* **3**, 013118 (2021).
- [36] A. Kubica, B. Yoshida, and F. Pastawski, Unfolding the color code, *New Journal of Physics* **17**, 083026 (2015).

- [37] H. Bombín, Gauge color codes: optimal transversal gates and gauge fixing in topological stabilizer codes, *New Journal of Physics* **17**, 083002 (2015).
- [38] H. Bombin, Transversal gates and error propagation in 3d topological codes (2018), [arXiv:1810.09575 \[quant-ph\]](https://arxiv.org/abs/1810.09575).
- [39] B. J. Brown, A fault-tolerant non-clifford gate for the surface code in two dimensions, *Science Advances* **6**, 10.1126/sciadv.aay4929 (2020).
- [40] M. E. Beverland, A. Kubica, and K. M. Svore, Cost of universality: A comparative study of the overhead of state distillation and code switching with color codes, *PRX Quantum* **2**, 020341 (2021).
- [41] I. Cong, H. Levine, A. Keesling, D. Bluvstein, S.-T. Wang, and M. D. Lukin, Hardware-efficient, fault-tolerant quantum computation with rydberg atoms, *Phys. Rev. X* **12**, 021049 (2022).
- [42] K. Sahay, J. Jin, J. Claes, J. D. Thompson, and S. Puri, High-threshold codes for neutral-atom qubits with biased erasure errors, *Phys. Rev. X* **13**, 041013 (2023).
- [43] Y. Wu, S. Kolkowitz, S. Puri, and J. D. Thompson, Erasure conversion for fault-tolerant quantum computing in alkaline earth rydberg atom arrays, *Nature Communications* **13**, 4657 (2022).
- [44] Q. Xu, J. P. B. Ataiades, C. A. Pattison, N. Raveendran, D. Bluvstein, J. Wurtz, B. Vasic, M. D. Lukin, L. Jiang, and H. Zhou, Constant-overhead fault-tolerant quantum computation with reconfigurable atom arrays (2023), [arXiv:2308.08648 \[quant-ph\]](https://arxiv.org/abs/2308.08648).
- [45] M. Barkeshli, Y.-A. Chen, P.-S. Hsin, and R. Kobayashi, Higher-group symmetry in finite gauge theory and stabilizer codes (2022), [arXiv:2211.11764 \[cond-mat.str-el\]](https://arxiv.org/abs/2211.11764).
- [46] M. Barkeshli, Y.-A. Chen, S.-J. Huang, R. Kobayashi, N. Tantivasadakarn, and G. Zhu, Codimension-2 defects and higher symmetries in (3+1)D topological phases, *SciPost Phys.* **14**, 065 (2023).
- [47] Y.-A. Chen and S. Tata, Higher cup products on hypercubic lattices: Application to lattice models of topological phases, *Journal of Mathematical Physics* **64**, 091902 (2023).

### A. Clifford errors in magic state distillation

In this appendix we discuss in some detail the effect of Clifford errors in magic state distillation of  $T$  ancilla. We use the  $[[15, 1, 3]]$  quantum Reed-Muller code with check matrix

$$\begin{aligned}
 H_X &= \begin{bmatrix} 1 & 0 & 1 & 0 & 1 & 0 & 1 & 0 & 1 & 0 & 1 & 0 & 1 & 0 & 1 \\ 0 & 1 & 1 & 0 & 0 & 1 & 1 & 0 & 0 & 1 & 1 & 0 & 0 & 1 & 1 \\ 0 & 0 & 0 & 1 & 1 & 1 & 1 & 0 & 0 & 0 & 0 & 1 & 1 & 1 & 1 \\ 0 & 0 & 0 & 0 & 0 & 0 & 0 & 1 & 1 & 1 & 1 & 1 & 1 & 1 & 1 \end{bmatrix}, \\
 H_Z &= \begin{bmatrix} 1 & 0 & 1 & 0 & 1 & 0 & 1 & 0 & 1 & 0 & 1 & 0 & 1 & 0 & 1 \\ 0 & 1 & 1 & 0 & 0 & 1 & 1 & 0 & 0 & 1 & 1 & 0 & 0 & 1 & 1 \\ 0 & 0 & 0 & 1 & 1 & 1 & 1 & 0 & 0 & 0 & 0 & 1 & 1 & 1 & 1 \\ 0 & 0 & 0 & 0 & 0 & 0 & 0 & 1 & 1 & 1 & 1 & 1 & 1 & 1 & 1 \\ 0 & 0 & 1 & 0 & 0 & 0 & 1 & 0 & 0 & 0 & 1 & 0 & 0 & 0 & 1 \\ 0 & 0 & 0 & 0 & 1 & 0 & 1 & 0 & 0 & 0 & 0 & 0 & 1 & 0 & 1 \\ 0 & 0 & 0 & 0 & 0 & 0 & 0 & 0 & 1 & 0 & 1 & 0 & 1 & 0 & 1 \\ 0 & 0 & 0 & 0 & 0 & 1 & 1 & 0 & 0 & 0 & 0 & 0 & 0 & 1 & 1 \\ 0 & 0 & 0 & 0 & 0 & 0 & 0 & 0 & 0 & 1 & 1 & 0 & 0 & 1 & 1 \\ 0 & 0 & 0 & 0 & 0 & 0 & 0 & 0 & 0 & 0 & 1 & 1 & 1 & 1 & 1 \end{bmatrix}, \tag{1}
 \end{aligned}$$

where each row in  $H_X$  defines an  $X$  stabilizer which has the identity operator  $I$  on sites with 0 while  $X$  on sites with 1. For example, the first row in  $H_X$  gives the stabilizer  $X_1 X_3 X_5 X_7 X_9 X_{11} X_{13} X_{15}$ . Similarly, rows in  $H_Z$  define the  $Z$  stabilizers. One logical qubit encoded in this code is

$$|\bar{0}\rangle = \prod_{i=1}^4 \frac{I + S_X^i}{\sqrt{2}} |00\dots 0\rangle, \quad |\bar{1}\rangle = \prod_{i=1}^4 \frac{I + S_X^i}{\sqrt{2}} |11\dots 1\rangle, \tag{2}$$

where  $S_X^i$  is the  $i$ th  $X$  stabilizer. It is straight forward to verify that

$$T^{\dagger \otimes 15} |\bar{0}\rangle = |\bar{0}\rangle, \quad T^{\dagger \otimes 15} |\bar{1}\rangle = e^{i\pi/4} |\bar{1}\rangle, \tag{3}$$

indicating that this code has a transversal logical  $T$  implementation via a bit-wise physical  $T^\dagger$  gate.

The detailed circuit for distillation is shown in Fig. 4. As discussed in the main text, we consider the major class of error, that is, the  $Z$  error on the CZ gates, which is modelled as

$$E(\rho) = CZ \left( (1-p)^2 \rho + p(I \otimes Z \rho I \otimes Z + Z \otimes I \rho Z \otimes I) + p^2 Z \otimes Z \rho Z \otimes Z \right) CZ^\dagger. \tag{4}$$

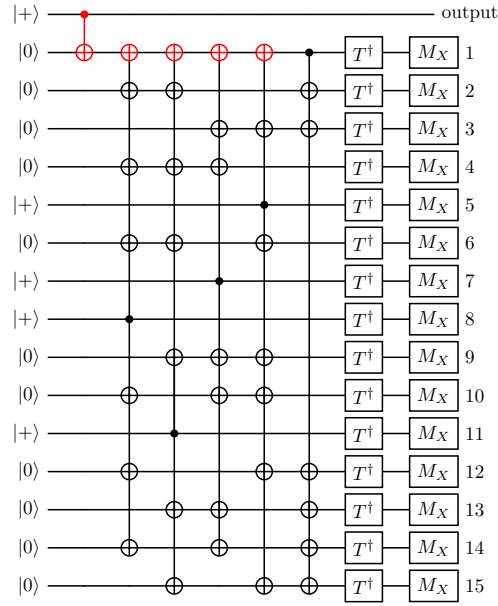


FIG. 4. Circuit for magic state distillation of  $T$  ancilla, adapted from [21]. The key gates,  $\text{CNOT}_{8,1}$ ,  $\text{CNOT}_{11,1}$ ,  $\text{CNOT}_{7,1}$ ,  $\text{CNOT}_{5,1}$  are labelled red.

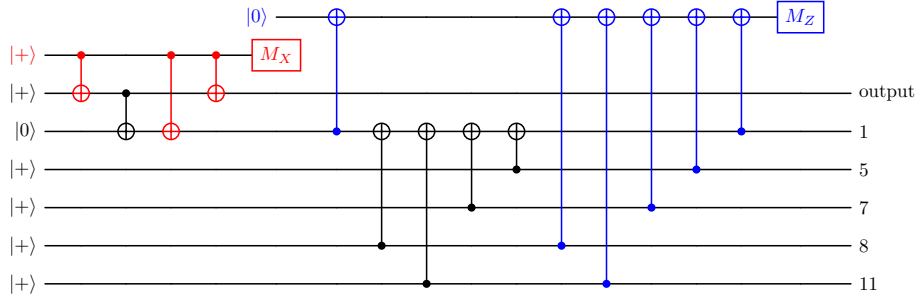


FIG. 5. Using flag qubit gadgets to detect errors on qubit 1 and the output qubit. Here only the relevant gates in the distillation circuit are shown. The flag qubit gadgets are colored red and blue respectively. If a  $Z$  error occurs on the output qubit, or an  $X$  error occurs on qubit 1 within the flag qubit gadgets, their corresponding flag qubit will be measured  $-1$  and this round of distillation should be discarded.

The Choi gate fidelity is  $F_{CZ} = (1 - p)^2$ . A  $\text{CNOT}$  gate can be obtained from a  $\text{CZ}$  gate by conjugating an  $H$  on the target qubit, which converts the  $Z$  error to an  $X$  one. In this error model, we see that

- The  $Z$  error on the control qubit when entangling the output qubit with qubit 1 will directly come into the final result, yielding a  $Z$  error.
- The five  $X$  errors on the target qubit 1 will be spread to qubits 1, 2, 3, 12, 13, 14, 15 as  $X_1 X_2 X_3 X_{12} X_{13} X_{14} X_{15}$  since  $\text{CNOT}(XI)\text{CNOT} = XX$ . Since  $T^\dagger X = e^{-i\pi/4} X S T^\dagger$ , where the factor is irrelevant while acting an  $X$  before measuring  $X$  has no effect, this error is equivalent to acting  $S^{\otimes 7}$  on the 7 qubits. A straightforward calculation using equation (2) shows that this is a logical  $S^\dagger$  gate, which will be teleported to the output qubit. An  $S^\dagger$  error with probability  $q$  contributes  $0.5q$  to the output error.
- Other errors, including those in implementing  $T^\dagger$  using noisy ancillae, are not spread, reducing linearly the rate of success while the contribution to the output error is at a higher order.

From the first two points, we see that if the gate fidelity is  $(1 - p)^2$ , the output qubit will be found with a  $Z$  error at probability  $p$ , and an  $S$  error at probability  $5p$ , yielding an output fidelity  $1 - 3.5p$ . Higher order contribution can come from two-qubit gates other than these 5 key gates.

### B. Fault-tolerant logical $C^{D-1}Z$ gates in $D$ -dimensional toric codes

This section introduces a simple method for topologically protected FT logical  $C^{D-1}Z$  gates in  $D$ -dimensional toric codes using physical  $C^{D-1}Z$  gates. As an example, we start with two layers of 2D toric codes on the square lattice. One logical  $\bar{X}_1$  gate in the first layer and another logical  $\bar{Z}_2$  in the second layer are

$$\bar{X}_1 = \cdots \begin{array}{|c|c|c|} \hline X_1 & X_1 & X_1 \\ \hline \end{array} \cdots, \quad \bar{Z}_2 = \cdots \begin{array}{|c|c|} \hline Z_2 & Z_2 \\ \hline \end{array} \cdots . \quad (5)$$

The CZ gate between logical qubits in the two different layers of toric codes is

$$\overline{CZ}_{1,2} = \cdots \begin{array}{|c|c|c|} \hline \vdots & \vdots & \vdots \\ \hline \begin{array}{|c|c|} \hline 2 & 2 \\ \hline \end{array} & \begin{array}{|c|c|} \hline 2 & 2 \\ \hline \end{array} & \\ \hline \begin{array}{|c|c|} \hline 1 & 1 \\ \hline \end{array} & \begin{array}{|c|c|} \hline 1 & 2 \\ \hline \end{array} & \begin{array}{|c|c|} \hline 2 & 2 \\ \hline \end{array} \\ \hline \begin{array}{|c|c|} \hline 1 & 1 \\ \hline \end{array} & \begin{array}{|c|c|} \hline 1 & 1 \\ \hline \end{array} & \\ \hline \vdots & \vdots & \vdots \\ \hline \end{array} \cdots , \quad (6)$$

the product of two physical CZ gates on each face, where the labels 1,2 indicate which layer it acts on. Two CZ gates correspond to two different paths from a corner of a square to the opposite corner.

This construction can be extended to three dimensions. Consider three layers of 3D toric codes. Logical  $X$  gates become membrane operators, while logical  $Z$  and CZ gates are the same as the 2D toric code. Define logical  $\bar{X}_3$  and logical  $\overline{CCZ}_{1,2,3}$  as

$$\bar{X}_3 = \cdots \begin{array}{|c|c|c|} \hline \vdots & \vdots & \vdots \\ \hline \begin{array}{|c|c|} \hline X_3 & X_3 \\ \hline \end{array} & \begin{array}{|c|c|} \hline X_3 & X_3 \\ \hline \end{array} & \begin{array}{|c|c|} \hline X_3 & X_3 \\ \hline \end{array} \\ \hline \begin{array}{|c|c|} \hline X_3 & X_3 \\ \hline \end{array} & \begin{array}{|c|c|} \hline X_3 & X_3 \\ \hline \end{array} & \begin{array}{|c|c|} \hline X_3 & X_3 \\ \hline \end{array} \\ \hline \vdots & \vdots & \vdots \\ \hline \end{array} \cdots , \quad (7)$$

$$\overline{CCZ}_{1,2,3} = \cdots \begin{array}{|c|c|c|} \hline \vdots & \vdots & \vdots \\ \hline \begin{array}{|c|c|} \hline 3 & 3 \\ \hline \end{array} & \begin{array}{|c|c|} \hline 3 & 3 \\ \hline \end{array} & \begin{array}{|c|c|} \hline 3 & 3 \\ \hline \end{array} \\ \hline \begin{array}{|c|c|} \hline 2 & 2 \\ \hline \end{array} & \begin{array}{|c|c|} \hline 2 & 2 \\ \hline \end{array} & \begin{array}{|c|c|} \hline 2 & 2 \\ \hline \end{array} \\ \hline \begin{array}{|c|c|} \hline 1 & 1 \\ \hline \end{array} & \begin{array}{|c|c|} \hline 1 & 1 \\ \hline \end{array} & \begin{array}{|c|c|} \hline 1 & 1 \\ \hline \end{array} \\ \hline \vdots & \vdots & \vdots \\ \hline \end{array} \cdots . \quad (8)$$

where logical  $\overline{\text{CCZ}}_{1,2,3}$  is the product of six  $\text{CCZ}$  gates in each cube. The labels 1, 2, 3 indicate which layer it acts on, and the six  $\text{CCZ}$  gates represent six paths from one corner to the opposite corner on a cube. One can verify that

$$\overline{\text{CCZ}}_{1,2,3} \overline{X}_3 \overline{\text{CCZ}}_{1,2,3} = \overline{X}_3 \overline{\text{CZ}}_{1,2}. \quad (9)$$

This construction applies to the  $D$ -dimensional hypercube directly, where  $\text{C}^{D-1}\text{Z}$  gates act on the edges of each path from one vertex to the opposite corner. In group cohomology language, the logical  $\overline{\text{CZ}}_{1,2}$  and  $\overline{\text{CCZ}}_{1,2,3}$  can be expressed by the cocycles  $\frac{1}{2}a_1 \cup a_2 \in H^2(\mathbb{Z}_2 \times \mathbb{Z}_2, \mathbb{R}/\mathbb{Z})$  and  $\frac{1}{2}a_1 \cup a_2 \cup a_3 \in H^3(\mathbb{Z}_2 \times \mathbb{Z}_2 \times \mathbb{Z}_2, \mathbb{R}/\mathbb{Z})$ . In  $D$  dimensions, the logical  $\text{C}^{D-1}\text{Z}$  gate corresponds to the cocycle  $\frac{1}{2}a_1 \cup a_2 \cup \dots \cup a_D \in H^D(\mathbb{Z}_2^D, \mathbb{R}/\mathbb{Z})$ . The details can be found in Refs. [45–47].